

Nanocarbons

Tridecacyclene Tetraimide: An Easily Reduced Cyclooctatetraene Derivative

Rakesh Kumar, Piotr J. Chmielewski, Tadeusz Lis, Dirk Volkmer, and Marcin Stępień*

Abstract: Tridecacyclene tetraimide, **TCTI**, an electron-deficient non-benzenoid nanocarbon with a $C_{56}N_4$ polycyclic framework was obtained in a concise synthesis. **TCTI** has a non-planar structure and forms π -stacked dimers in the solid state. In solution, it undergoes eight single-electron reductions, yielding a range of negatively charged states up to an octaanion. Except for the latter species, which has a remarkably large electronic gap, the anions feature extended near-infrared absorptions, with a particularly strong band at 1692 nm observed for the dianion. A computational analysis of the **TCTI** anions shows that their stability originates from the combined effects of electron-deficient imide groups and the local aromaticity of reduced acenaphthylene units. The properties of **TCTI** make it potentially useful in electrochromic and charge storage applications.

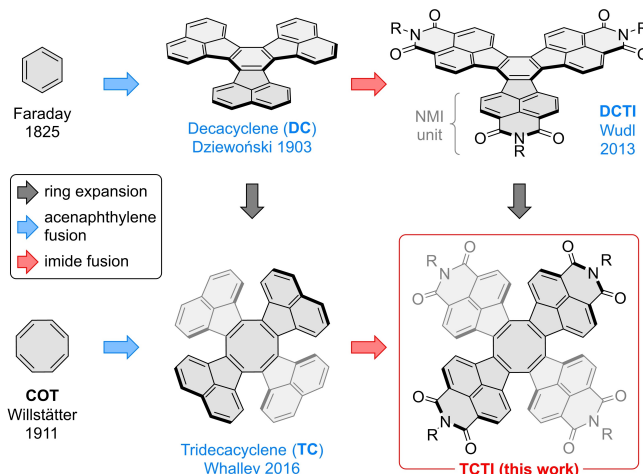


Figure 1. Structural design of tridecacyclene tetraimide (**TCTI**).

Introduction

Expansion of aromatic systems via peripheral fusion of acenaphthylene units has been recognized as an efficient strategy for development of organic semiconductors and chromophores.^[1–4] Decacyclene (**DC**, Figure 1), discovered by Rehländer and Dzewoński more than a century ago,^[5,6] may be viewed as an early prototype of such an acenaphthylene-fused system. Decacyclene and its derivatives have enjoyed recent interest as chiral aromatics,^[7] organometallic ligands,^[8–10] self-assembling materials,^[11–14] open-shell organics,^[15] and precursors of curved nanocarbons.^[16–19] Among these systems, Wudl's decacyclene triimide^[14] (**DCTI**, Figure 1) provides a notable example of an electron-deficient system containing peripherally fused naphthali-

imide (NMI) fragments. Expansion of aromatic nanocarbons via peripheral NMI fusion has been widely applied to benzenoid,^[20–22] non-benzenoid,^[23–26] and heterocyclic targets,^[27–33] providing access to multi-electron acceptors, near-infrared absorbers, and non-planar aromatics.

The properties of such systems heavily depend on the choice of the core motif that is subjected to NMI extension. For instance, the azulene-containing isomer of terrylene diimide features a drastically reduced electronic gap,^[25] whereas oligopyrrole-based cores have been found to enable multiple reversible reductions to produce highly charged oligoanions.^[27,28] Looking for a compact core motif that could be densely decorated with NMI units, we turned our attention to the hitherto unknown tridecacyclene tetraimide (**TCTI**, Figure 1), the higher homologue of **DCTI**. The parent tridecacyclene (**TC**), discovered in 2016 by Whalley et al.,^[34,35] can be reduced to the corresponding mono- and dianion at relatively low potentials, but its chemistry has remained relatively unexplored. While some π -extended **TC** derivatives are known,^[36,18,37] functionalization of tridecacyclene has not been reported, possibly because of its unfavorable reactivity, e.g. susceptibility to rearrangement.^[38]

TCTI can be viewed as a quadruply NMI-fused derivative of 1,3,5,7-cyclooctatetraene (**COT**).^[39,40] The **COT** motif has been elaborated into a variety of planarized derivatives,^[41] saddle-shaped heteroaromatics,^[42–49] and negatively curved nanocarbons,^[50–52] providing access to hole transporters,^[46] AIE materials,^[47] and as-cast solar cells.^[49] **COT**^[53] and its π -extended analogues^[35,54–57] can be reduced

[*] Dr. R. Kumar, Prof. P. J. Chmielewski, Prof. T. Lis, Prof. M. Stępień
 Wydział Chemii, Uniwersytet Wrocławski
 ul. F. Joliot-Curie 14, 50-383 Wrocław (Poland)
 E-mail: marcin.stepien@uwr.edu.pl

Prof. Dr. D. Volkmer
 Institute of Physics, Chair of Solid State and Materials Science,
 Augsburg University
 Universitätsstrasse 1, 86159 Augsburg (Germany)

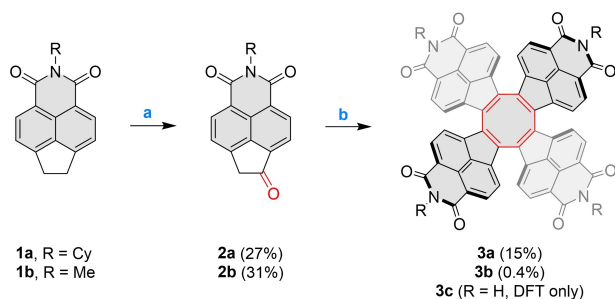
© 2022 The Authors. Angewandte Chemie International Edition published by Wiley-VCH GmbH. This is an open access article under the terms of the Creative Commons Attribution Non-Commercial NoDerivs License, which permits use and distribution in any medium, provided the original work is properly cited, the use is non-commercial and no modifications or adaptations are made.

to a variety of anionic states, in particular the aromatically stabilized dianion.^[58,59] In the present work, the combination of the COT ring with electron-withdrawing peripheries is shown to result in a relatively small π system that is susceptible to eight-fold reduction and yields anionic species with remarkable absorptions in the near-infrared range.

Results and Discussion

TCTI was obtained as a cyclohexyl-substituted derivative **3a** using the procedure shown in Scheme 1. First, the regioselective mono-oxidation of acenaphthene imide **1a** with CrO₃ in acetic anhydride produced the corresponding acenaphthone **2a**. The latter intermediate was refluxed with TiCl₄ in *o*-dichlorobenzene for three hours, providing the desired tridecacyclene tetraimide **3a** in 15% yield and no corresponding DCTI (for details, see the Supporting Information). The low yield of this condensation reaction can be attributed to the formation of polymeric byproducts and, possibly, higher cyclic oligomers,^[37] which however were not detectable in the crude reaction mixtures. For the methyl-substituted ketone **2b**, the yield of the desired **3b** was much lower (0.4%), possibly reflecting the very low solubility of the starting material in *o*-dichlorobenzene.

Under similar conditions, 1-acenaphthone itself was previously found to yield 21% of tridecacyclene along with traces of decacyclene,^[34] a result we were able to reproduce in our laboratory. Interestingly, a preference for decacyclene formation had been observed in earlier work by Moszew and Żankowska-Jasińska under protic condensation conditions^[60] and by Scott et al., who used the TiCl₄-catalyzed protocol.^[61] The origin of these differences in ring-size selectivity is not clear; however, it can be reasonably expected that the outcome of the condensation may depend on the functionalization of 1-acenaphthone, steric congestion, and fine details of reaction conditions. In particular, water content in the reaction mixtures may affect the kinetics and reversibility of condensation. Decacyclene could be expected to be the thermodynamic product, given (a) its greater aromatic stabilization and (b) the typical reactivity patterns of cyclic ketones in aldol self-condensations.^[62] The formation of tridecacyclene might therefore indicate a kinetically controlled condensation,



Scheme 1. Synthesis of **3a** and **3b**. Reagents and conditions:

a) chromium(VI) oxide (1.5 equiv), acetic anhydride, rt, 4–5 h; b) TiCl₄ (6.0 equiv), *o*-dichlorobenzene, reflux, 3 h.

possibly involving two molecules of the initially formed biacenone.^[60,61]

The TCTI derivatives were characterized by NMR spectroscopy and mass spectrometry (see the Supporting Information). Additionally, the structure of **3a** was confirmed by X-ray crystallography (Figures 2A, B, and S6).^[63] The brown-colored single crystals of **3a** were grown by slow vapor diffusion of methanol into a solution of **3a** in 1,2-dichloroethane. In the crystal, two symmetry-independent molecules of **3a** were found, both having the expected tub-shaped conformation characteristic of COT derivatives. Double bonds of the COT moiety are localized in the five-membered rings (as shown in Scheme 1), as previously observed for the parent TC hydrocarbon.^[34] Crystallographically determined average double and single bond lengths in the COT fragment of **3a** are 1.381(7) Å and 1.459(10) Å, respectively (cf. 1.369 Å and 1.470 Å reported for TC). Both molecules of **3a** showed however a notable distortion from the idealized D_{2d} symmetry, with markedly different interplanar angles between the opposite acenaphthyleneimide moieties (90.8°, 114.8° and 90.2°, 112.0°, vs. 103–105° in TC^[34]). The distortion is apparently caused by the formation of a non-covalent dimer in the solid state (Figures 2C and D). The dimer has an approximate C_2 symmetry and features a π - π interaction between two acenaphthyleneimide units, which are aligned at a torsional angle of ca. 77° along

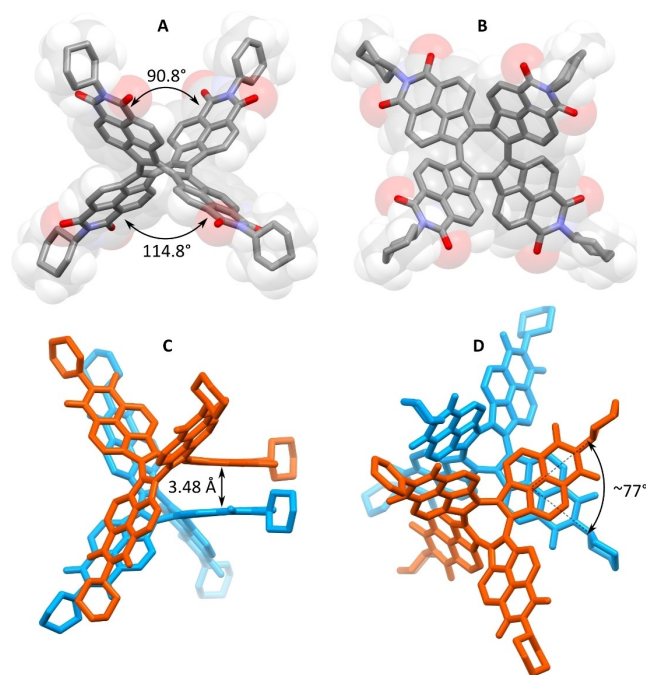


Figure 2. Molecular structure of **3a** determined in an X-ray diffraction analysis (solvent molecules and hydrogens are omitted for clarity). A) and B) Side and top views of one of two symmetry-independent molecules of **3a** present in the crystal lattice. Splay angles between mean planes of nonadjacent acenaphthyleneimide units are indicated in panel A. C) and D) Non-covalent dimer formed by two molecules of **3a** (red and blue respectively) in the solid state. The centroid-to-plane distance is calculated between overlapping acenaphthyleneimide units of the two molecules.

the stacking direction. The stacking distance of ca. 3.48 Å is remarkably small for such a highly non-planar structure. No other π -stacking interactions were however not observed in the crystal, possibly being suppressed by the relatively bulky cyclohexyl groups. This assumption is in line with the apparently weak aggregation of **3a** in solution, which is inferred from the insignificant concentration dependence of ^1H NMR shifts (in CDCl_3). Appropriate selection of the imide R substituents may however lead to TCTI derivatives characterized by extended π - π interaction networks in the solid state, which might result in favorable charge-transport properties.

3a showed a strikingly rich redox behavior in electrochemical experiments (Figure 3). In particular, it readily undergoes eight one-electron reductions in the -0.88 to -2.71 V potential range (vs. Fc^+/Fc). One irreversible oxidation event at ca. 1.01 V was also observed, indicating that the electrochemical energy gap of **3a** (ca. 1.89 eV) is only slightly diminished relative to that of **TC** (2.11 eV).^[34] A chronocoulometric analysis carried out for **3a** at -2.3 V indicated the transfer of 5.5 ± 0.2 electrons, further confirming the one-electron character of the first six reductions (Supporting Information). In comparison, the reported electrochemical response of **DCTI** was rather poorly resolved with no observable oxidation and a reduction onset at ca. -1.2 V (in *o*-dichlorobenzene).^[14] The imide-free decacyclene (**DC**) could be reduced to the tetraanion at very low potentials ($E_{\text{red4}} = -3.31$ V vs. Ag/AgNO_3 in 1,2-dimethoxyethane)^[64] whereas only two reductions were observed for **TC** above -2.5 V (vs. Fc^+/Fc in acetonitrile).^[35] The behavior of **3a** is thus a consequence of the simultaneous presence of the COT and NMI substructures in the molecule, and resembles the extended redox activity of porphyrin- and azacoronene-based oligoimides.^[27,28]

In line with the above electrochemical data, **3a** is susceptible to two reduction steps when treated with cobaltocene (CoCp_2 , $E^{\circ} = -1.3$ V^[65]), as revealed in a UV/Vis-NIR titration experiment (Figure 4A). The electronic absorption spectrum of the neutral **3a** contains an intense

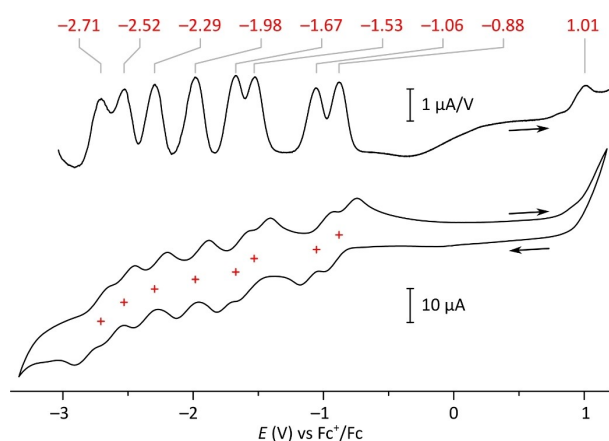


Figure 3. Cyclic voltammogram (bottom) and differential pulse voltammogram (top) recorded for compound **3a** (THF, $[\text{Bu}_4\text{N}]\text{PF}_6$, glassy-carbon electrode, 100 mV s^{-1}).

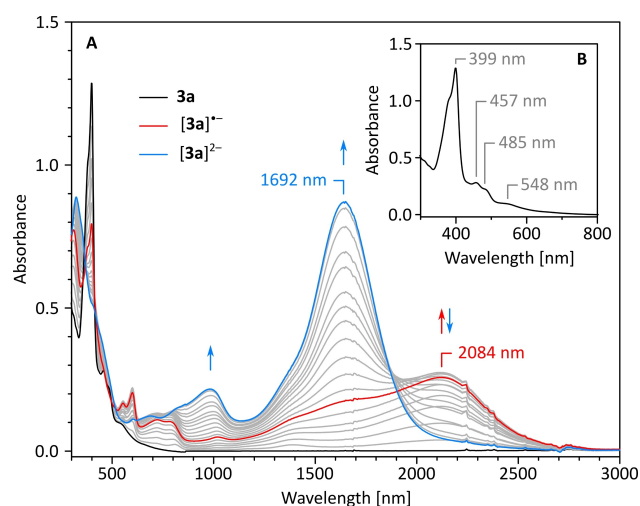


Figure 4. A) Stepwise reduction of **3a** (0.166 mM in CH_2Cl_2) with cobaltocene (1.66 mM in CH_2Cl_2). The red and blue traces correspond to the maximum concentration of $[\mathbf{3a}]^{\bullet-}$ and $[\mathbf{3a}]^{2-}$, respectively. B) Expansion of the absorption spectrum of **3a**.

band at 399 nm and several weaker features at longer wavelengths, with a weak absorption tail extending beyond 700 nm (Figure 4B). When treated with CoCp_2 in an inert atmosphere of the glove-box, **3a** initially produced a broad NIR absorption with a maximum at 2084 nm, which was ascribed to the **TCTI** radical anion, $[\mathbf{3a}]^{\bullet-}$. Further addition of CoCp_2 (up to 6.0 equiv) yielded another NIR-absorbing species, presumed to be the dianion $[\mathbf{3a}]^{2-}$, which was characterized by a prominent absorption band at 1692 nm. The above assignments were confirmed using thin-layer spectroelectrochemistry, which produced similar absorption profiles at the first two reduction potentials (Figure S5).

No isosbestic points were observed in the CoCp_2 titration, indicating that $[\mathbf{3a}]^{\bullet-}$ and $[\mathbf{3a}]^{2-}$ coexist in solution, in line with the small difference of E_{red1} and E_{red2} potentials (0.18 V). The reversibility of chemical reductions was further demonstrated in a comproportionation experiment, in which $[\mathbf{3a}]^{\bullet-}$ was formed by mixing solutions of **3a** and $[\mathbf{3a}]^{2-}$ (Figure S1). The dianion obtained in reaction with CoCp_2 was reoxidized back to the neutral species with exposure to air. In the course of titration, the color of the solution changes from yellowish (**3a**), through greenish-brown ($[\mathbf{3a}]^{\bullet-}$), to olive-green ($[\mathbf{3a}]^{2-}$). However, solutions of **3a** retain much of their visible-light transparency upon reduction and all major spectral changes occur in the NIR range. **TCTI** derivatives could thus potentially be implemented in electrochromic switches to provide NIR opacity over a wide range of wavelengths.

To obtain higher $[\mathbf{TCTI}]^{n-}$ anions ($n > 2$), we treated **3a** with more potent reducing agents than CoCp_2 . Exposure of **3a** to excess metallic sodium in THF produced only the dianionic $[\mathbf{3a}]^{2-}$ after 17 hours. Further reduction could however be achieved using sodium naphthalenide (NaN) in THF in the presence of 15-crown-5 (Figures 5A–C and S2–S4). Initial titration steps (up to 3.5 nominal equiv of NaN) produced the previously observed $[\mathbf{3a}]^{\bullet-}$ and $[\mathbf{3a}]^{2-}$. Further

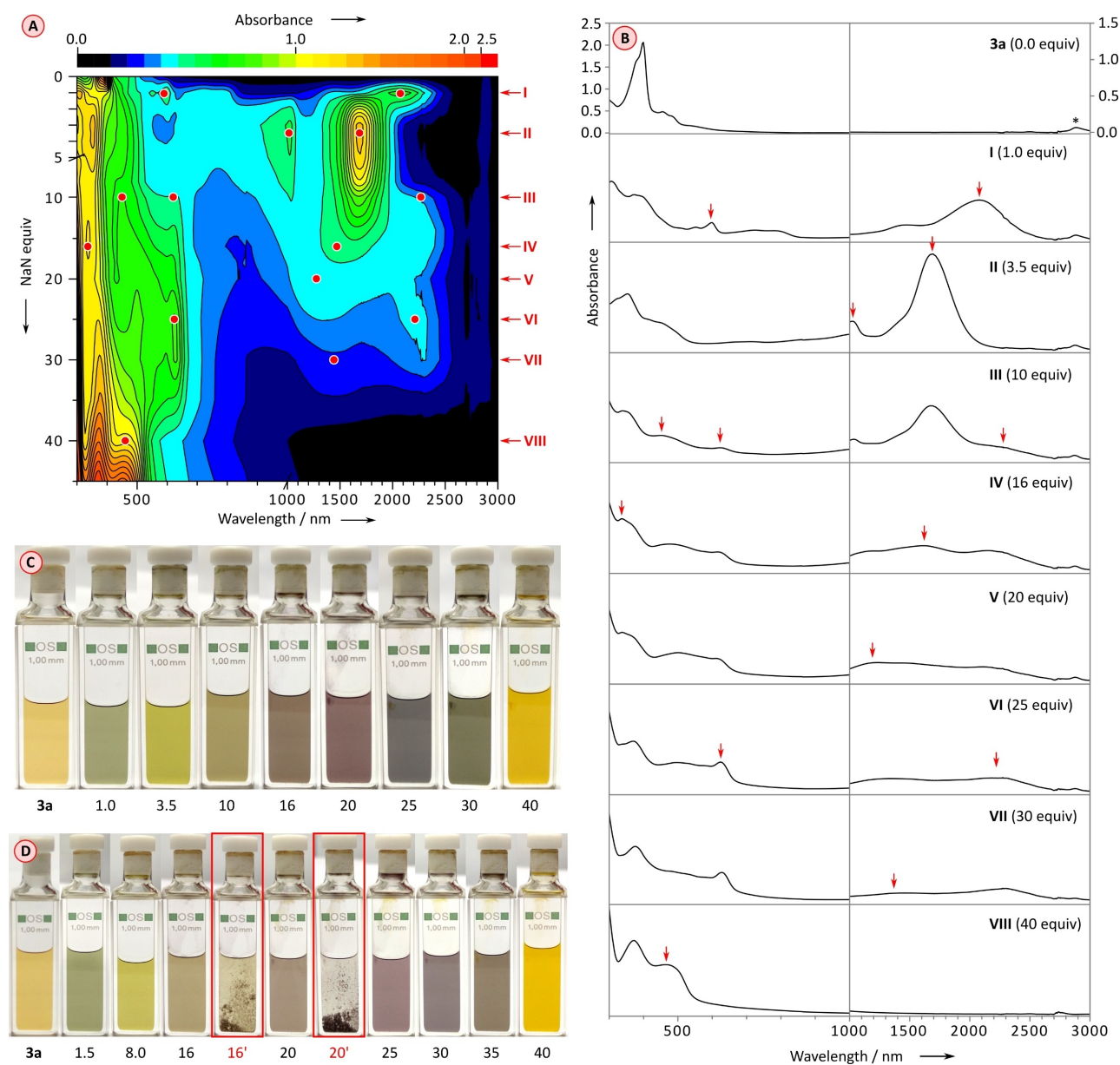


Figure 5. Chemical reduction of **3a** with sodium naphthalenide (NaN) monitored using UV/Vis-NIR absorption spectroscopy (0.25 mM **3a** in THF, nominal equiv of NaN corresponding to the initial concentration of naphthalene). A)–C) Behavior observed in the presence of 15-crown-5 (80 equiv added to the initial solution). Spectral features of interest are indicated with red dots and arrows in (A) and (B), respectively. D) Behavior observed in the absence of the crown ether.

addition of NaN resulted in gradual changes in the NIR region of the absorption spectrum, resembling those previously reported for other highly reduced NMI-fused aromatics.^[27,28] The broad and overlapping bands make it difficult to identify specific anionic states, however, the emergence of multiple maxima can be correlated with up to eight distinct species (Figures 5A and B). The endpoint of the titration was reached at ca. 40 equiv of added NaN, and no further spectral changes were observed beyond this point. Remarkably, in the ultimate titration stage, which corresponds to the deep yellow color of the solution, no bands are observed above 1000 nm, suggesting that the final reduced state may be characterized by a relatively large

electronic gap. The latter species, which was assumed to be the octaanion [**3a**]⁸⁻ (see below), could be reoxidized to the neutral **3a** by addition of diiodine in tetrahydrofuran.

The complexity of reduction chemistry of **3a** was further demonstrated by a NaN titration performed in the absence of the crown ether additive (Figure 5D). The behavior of **3a** was essentially identical up to 16 equiv of added NaN, at which point a dark solid precipitated from the solution after 10 minutes. The solid was temporarily redissolved upon addition of further 4 equiv of NaN, but a precipitate reappeared after ca. 10 min. Further addition of NaN resulted in dissolution of the solid, and subsequent spectral changes were identical with those observed in the presence

of 15-crown-5. The formation of the solid may be tentatively ascribed to formation of polymeric π complexes between sodium cations and specific $[\mathbf{3a}]^{n-}$ anions, possibly with $n=4$ to 5. Apparently the aggregation is less extensive for both lower and higher reduced states of $\mathbf{3a}$, and the precipitation can be completely suppressed by crown ether complexation of Na^+ .

Density functional theory (DFT) was used to probe the properties of **TCTI** as a function of its oxidation level. These calculations were performed for the substituent-free derivative **3c** (Scheme 1) at the conventional B3LYP/6-31G(d,p) level of theory, to obtain a preliminary, qualitative picture of changes occurring upon charging of **TCTI**. However, quantitative accuracy cannot be expected, given the inherent difficulties in accurate theoretical modeling of highly charged anions in general, and **COT** anions in particular.^[58,59] The optimized gas-phase geometry of the neutral **3c** had the expected D_{2d} -symmetric conformation, and reproduced the solid-state bonding distances with very good precision (see Supporting Information for Cartesian coordinates). Kohn–Sham HOMO and LUMO levels of **3c** are non-degenerate with an energy gap of 2.06 eV (Figure 5A). Importantly, the four lowest virtual levels (LUMO through L+3, -3.99 to -3.36 eV) are significantly more stabilized than the next higher level (L+4, -1.55 eV). This feature^[27,28] is consistent with the accessibility of eight reductions in **TCTI**. In comparison, Wudl's **DTI** features a larger KS energy gap (2.97 V) and three low-lying unoccupied levels, which are however less stabilized (-3.49 , -3.47 , and -3.25 V). These differences are quite significant for two homologs and may be linked to the disparate aromatic characters of the COT and benzene rings, respectively.

All even-electron anions $[\mathbf{3c}]^{n-}$ ($n=2, 4, 6, \text{ and } 8$) were found to be ground-state singlets, with stable closed-shell wavefunctions obtained for $n=2$ and 8. Broken-symmetry

open-shell singlets were found for $n=4$ and 6, apparently reflecting the small energy spacings among L+1, L+2 and L+3 orbitals of **3c**. All $[\mathbf{3c}]^{n-}$ anions retained the tub conformation of the neutral species, with only slight deviations from the ideal D_{2d} symmetry observed for $n=3, 4, 5, \text{ and } 6$. The anions show similarly symmetrical distributions of Mulliken charges (Table S3), indicating that for each oxidation state, the anionic charge is uniformly distributed among all NMI subunits.

In the DFT geometries, bonding distances within the π -conjugated **TCTI** core of $[\mathbf{3c}]^{n-}$ undergo characteristic changes with the increasing negative charge. The formal single and double bonds of the COT ring (**a** and **b** respectively, Figure 6B) show the most interesting behavior, i.e., they undergo partial equalization on going from $n=0$ (1.462 and 1.385 Å) to $n=2$ (1.443 and 1.416 Å). For higher negative charges, the equalization is less pronounced than in the dianion, but progressive lengthening of both bond types is observed. Monotonic lengthening is also observed for imide C=O bonds (**e**), whereas then nominally single bonds **c** and **d** are gradually shortened with the increasing negative charge. The saddle distortion of the **COT** unit in $[\mathbf{3c}]^{n-}$ is only slightly affected by the increasing anion charge. In most cases, the splay angles between opposite acenaphthyleneimide units are equal and range from 102.17° ($n=0$) to 108.46° ($n=2$), with unequal splay angles observed for $n=3$ ($104.58^\circ, 110.58^\circ$) and $n=5$ ($108.20^\circ, 107.42^\circ$).

Energy gaps obtained from DFT calculations are in qualitative agreement with the experiment. Specifically, Kohn–Sham HOMO–LUMO gaps are very small in the $[\mathbf{3c}]^{n-}$ anions ($n=1$ through 7, 0.40–1.07 V), consistent with the experimentally observed NIR absorptions of these species. Remarkably, a much larger gap of 2.96 eV is predicted for the octaanion, $[\mathbf{3c}]^{8-}$. Thus, the disappearance of NIR maxima in the ultimate steps of NaN titration of **3a** may indicate that the octaanion state was indeed reached under those conditions. Electronic spectra of $[\mathbf{3c}]^{n-}$ states obtained from time-dependent (TD) DFT simulations corresponded well with the experimental data for $n=0, 1, 2$ and 8 (see the Supporting Information). The accuracy of TD-DFT calculations could not be verified for other anions, because they were not observed as discrete species in the titration experiments, however, all of these species were predicted to absorb strongly in the 1000 to 3000 nm range.

π -Electron delocalization and its magnetic manifestations were further probed for selected redox states of **3c** using anisotropy of induced current density (ACID),^[66] and nucleus-independent chemical shift (NICS)^[67] calculations (Figure 7). For the neutral **3c**, the ACID plot revealed strong clockwise circulations in the four naphthalene subunits and a weak anticlockwise current in the COT ring. Interestingly, $[\mathbf{3c}]^{2-}$ showed a qualitatively similar ACID plot, with somewhat diminished naphthalene ring currents. In $[\mathbf{3c}]^{8-}$ however, delocalization enhancement was observed in each acenaphthyleneimide unit, with a dominant clockwise current circulating in the five-membered ring. A 2D NICS map obtained for the neutral **3c** confirmed the dominant contribution of naphthalene diatropicity, whereas the inner deshielding of the 8-membered ring turned out to

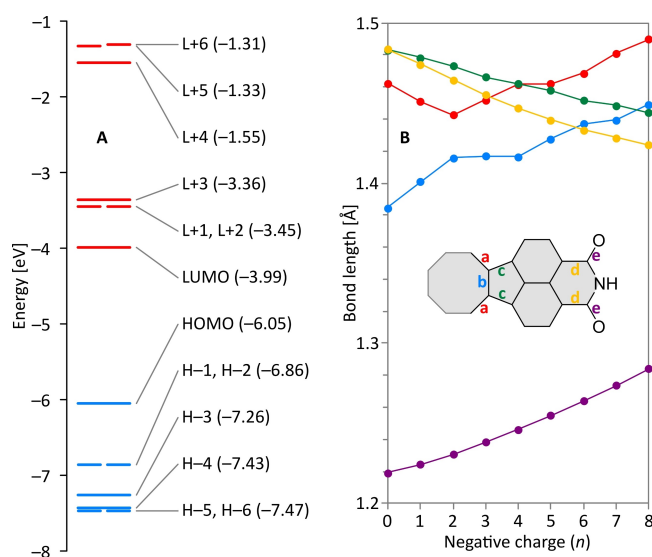


Figure 6. A) Kohn–Sham frontier molecular orbitals of **3c** (B3LYP/6–31G(d,p)). B) Charge dependence of selected bond lengths in $[\mathbf{3c}]^{n-}$ ($n=0$ to 8). Distances correspond to optimized DFT geometries and are symmetry-averaged.

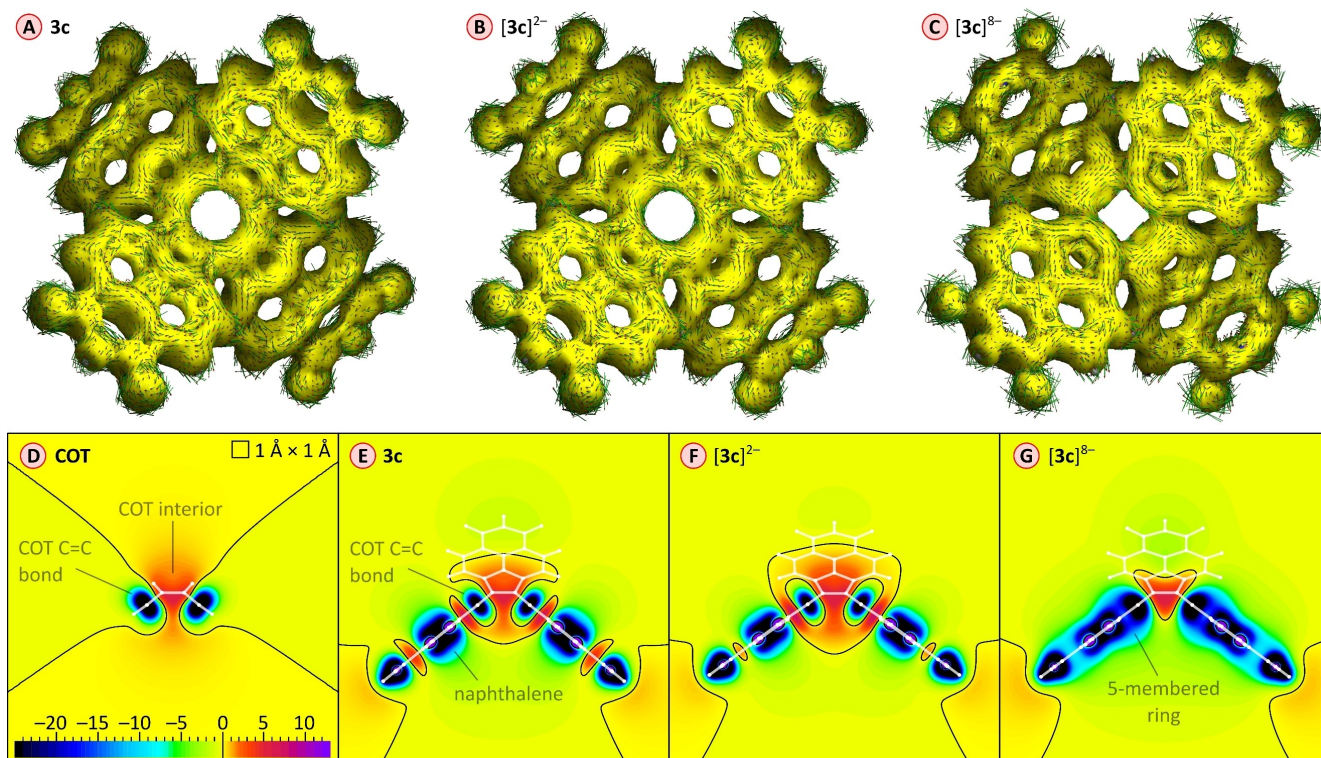


Figure 7. A)–C) ACID plots for **3c**, **[3c]²⁻**, and **[3c]⁸⁻** (CSGT for B3LYP/6–31G(d,p) densities and geometries, 0.03 a.u. isosurface value, magnetic field vector oriented perpendicular to the viewing plane). Note the increase of the ACID density in the five-membered rings of **[3c]⁸⁻**. D)–G) NICS maps for **COT**, **3c**, **[3c]²⁻**, and **[3c]⁸⁻** based on isotropic GIAO/B3LYP/6–31G(d,p) shieldings. Cross-sections were taken through the geometrical center of each system, along one of the σ_d symmetry planes passing through two double bonds (**COT**) or two NMI units (**[3c]ⁿ⁻**). Molecular structures are superimposed as transparent stick models. Gray labels indicate the positions of key molecular fragments and associated ring currents.

be comparable in magnitude with that of the isolated COT ring (Figures 7F vs. E). In **[3c]²⁻**, naphthalene fragments are somewhat less diatropic, while the COT deshielding zone is relatively unaffected, in line with the ACID data. The NICS plot obtained for **[3c]⁸⁻** shows that each acenaphthyleneimide subunit becomes more strongly diatropic. The strongest current is observed in the five-membered ring, again confirming the predictions of the ACID method.

Taken together, the computational data show that charging of **TCTI** occurs without large-scale geometrical changes. This structural rigidity is apparently a consequence of the steric bulk introduced by quadruple acenaphthylene fusion. In fact, the tridecacyclene dianion **[TC]²⁻** was reported to have a saddle shape similar to that of **[3c]²⁻**.^[35] This structural preference contrasts with the planarity of the **[COT]²⁻** dianion^[59] and isomerization observed recently for a tetrabenzo derivative.^[57] Because of the nonplanarity, the COT ring in **[3c]²⁻** is not diatropic, however, it displays geometrical changes (bond equalization and flattening) that are specific to this particular oxidation level of **TCTI** and are consistent with residual 10-electron aromaticity. The slight changes of magnetism associated with this local aromatic character are likely obscured by the more pronounced diatropic contributions of the surrounding rings.

Bond length variations in the higher **[3c]ⁿ⁻** anions ($n > 2$) imply that the increasing negative charge becomes progres-

sively more localized on the oxygens of the NMI subunits, leading to a decrease of the CO bond order (bond **e**, Figure 6B). Such a placement of the negative charge can be described in terms of the quinoidal resonance structure **I** (Figure 8). Its increasing contribution is also consistent with the observed shortening of bonds **c** and **d**. In particular, in **[3c]⁸⁻**, the acenaphthylene bond **c** (1.444 Å) is shorter than the **COT** bonds **a** and **b** (1.490 Å and 1.449 Å, respectively), indicating a certain degree of [8]radialene character. Radialene conjugation alone does not, however, explain the distinct diatropicity of acenaphthyleneimide units in **[3c]⁸⁻**. Their aromaticity combines features of the cyclopentadienyl anion and acenaphthylene dianion^[68] and can be rationalized

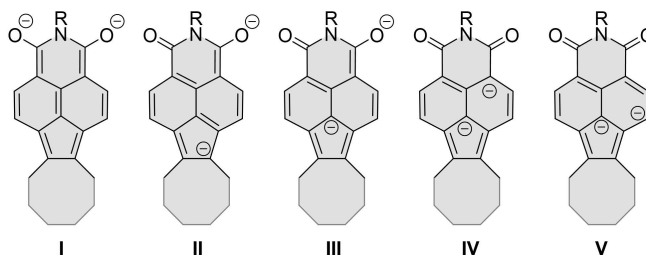


Figure 8. Dianionic resonance contributions to π -conjugation in **[TCTI]ⁿ⁻** oligoanions.

using resonance structures in which one or two negative charges are placed within the acenaphthylene moiety (e.g., **II** through **V**, Figure 8).

Conclusion

Tridecacyclene tetraimide described in this work comprises four naphthalimide units fused to a central cyclooctatetraene ring. Such a design yields an electron-deficient π -system that is susceptible to eight reversible one-electron reductions, which can be induced using both chemical and electrochemical methods. Anions obtained upon reduction absorb strongly in the near infrared, with a particularly intense band displayed by the dianion. These remarkable electronic characteristics are specific to the particular combination of electron-withdrawing functionalities and non-benzenoid fusion, since they are absent in the parent tridecacyclene and in the homologous benzene-based triimide. The combination of negative curvature and π -stacking in the solid state indicates the potential of **TCTI** derivatives for creating extended π - π interaction networks with enhanced charge-transport properties.^[69–71]

Our computational analysis shows that the stabilization of **TCTI** oligoanions is caused by a combination of several factors, including (a) the electron-withdrawing nature of imide functionalities, which lowers the energies of frontier unoccupied MOs, (b) local aromaticity gained by acenaphthyleneimide units upon reduction, and (c) charge delocalization over multiple NMI subunits, contributing particularly to the stabilization of intermediate reduced states ($n < 8$). This interpretation may be applicable to other related systems, including NMI-fused oligopyrroles,^[27,28] and provides useful hints on designing easily reducible nanocarbons. In particular, it rationalizes the importance of acenaphthylene fusion, and the role of the core motif, which can be as small as the COT ring, as long as it ensures efficient electronic communication among the electron-deficient subunits. We are currently investigating further implications of these design principles.

Acknowledgements

Financial support was kindly provided as part of the Polish-German BEETHOVEN CLASSIC program funded jointly by the National Science Center of Poland (UMO-2018/31/G/ST5/01813, to M.S.) and the German Science Foundation (DFG, VO 829/14-1, to D.V.). Theoretical calculations were performed using the resources provided by the Wrocław Center for Networking and Supercomputing.

Conflict of Interest

The authors declare no conflict of interest.

Data Availability Statement

The data that support the findings of this study are available in the Supporting Information of this article.

Keywords: Annulenes · Aromaticity · Nanocarbons · Redox Chemistry · Structure Elucidation

- [1] Y.-H. Liu, D. Perepichka, *J. Mater. Chem. C* **2021**, *9*, 12448–12461.
- [2] T. D. Lash, P. Chandrasekar, *J. Am. Chem. Soc.* **1996**, *118*, 8767–8768.
- [3] M. Stępień, E. Gońka, M. Żyła, N. Sprutta, *Chem. Rev.* **2017**, *117*, 3479–3716.
- [4] A. Borisso, Y. K. Maurya, L. Moshniaha, W.-S. Wong, M. Żyła-Karwowska, M. Stępień, *Chem. Rev.* **2022**, *122*, 565–788.
- [5] K. Dziewoński, *Bull. Int. Acad. Sci. Cracovie* **1903**, *2*, 77–82.
- [6] P. Rehländer, *Ueber einige Azoline der Anissäurereihe: Ueber das Binaphthylthiophen und das Trinaphthylbenzol*, A. W. Schade's Buchdruckerei, Berlin, **1893**.
- [7] X. Geng, J. T. Mague, R. A. Pascal, *J. Org. Chem.* **2015**, *80*, 4824–4827.
- [8] M. Munakata, L. P. Wu, G. L. Ning, T. Kuroda-Sowa, M. Maekawa, Y. Suenaga, N. Maeno, *J. Am. Chem. Soc.* **1999**, *121*, 4968–4976.
- [9] H. Bock, K. Gharagozloo-Hubmann, S. Holl, M. Sievert, *Z. Naturforsch. B* **2000**, *55*, 1163–1178.
- [10] J. J. Schneider, D. Spickermann, C. W. Lehmann, J. Magull, H.-J. Krüger, J. Enslin, P. Gütllich, *Chem. Eur. J.* **2006**, *12*, 1427–1435.
- [11] E. Keinan, S. Kumar, R. Moshenberg, R. Ghirlando, E. J. Wachtel, *Adv. Mater.* **1991**, *3*, 251–254.
- [12] C. Li, Q. Zeng, P. Wu, S. Xu, C. Wang, Y. Qiao, L. Wan, C. Bai, *J. Phys. Chem. B* **2002**, *106*, 13262–13267.
- [13] K. Hirota, K. Tajima, K. Hashimoto, *Synth. Met.* **2007**, *157*, 290–296.
- [14] T. V. Pho, F. M. Toma, M. L. Chabynec, F. Wudl, *Angew. Chem. Int. Ed.* **2013**, *52*, 1446–1451; *Angew. Chem.* **2013**, *125*, 1486–1491.
- [15] T. Kubo, K. Yamamoto, K. Nakasuji, T. Takui, I. Murata, *Angew. Chem. Int. Ed. Engl.* **1996**, *35*, 439–441; *Angew. Chem.* **1996**, *108*, 456–457.
- [16] L. T. Scott, M. S. Bratcher, S. Hagen, *J. Am. Chem. Soc.* **1996**, *118*, 8743–8744.
- [17] L. T. Scott, M. M. Boorum, B. J. McMahon, S. Hagen, J. Mack, J. Blank, H. Wegner, A. de Meijere, *Science* **2002**, *295*, 1500–1503.
- [18] T. J. Hill, R. K. Hughes, L. T. Scott, *Tetrahedron* **2008**, *64*, 11360–11369.
- [19] J. R. Sanchez-Valencia, T. Dienel, O. Gröning, I. Shorubalko, A. Mueller, M. Jansen, K. Amsharov, P. Ruffieux, R. Fasel, *Nature* **2014**, *512*, 61–64.
- [20] S. Seifert, K. Shoyama, D. Schmidt, F. Würthner, *Angew. Chem. Int. Ed.* **2016**, *55*, 6390–6395; *Angew. Chem.* **2016**, *128*, 6500–6505.
- [21] B. Liu, M. Bockmann, W. Jiang, N. L. Doltsinis, Z. Wang, *J. Am. Chem. Soc.* **2020**, *142*, 7092–7099.
- [22] G. Liu, C. Xiao, F. Negri, Y. Li, Z. Wang, *Angew. Chem. Int. Ed.* **2020**, *59*, 2008–2012; *Angew. Chem.* **2020**, *132*, 2024–2028.
- [23] D. Meng, G. Liu, C. Xiao, Y. Shi, L. Zhang, L. Jiang, K. K. Baldrige, Y. Li, J. S. Siegel, Z. Wang, *J. Am. Chem. Soc.* **2019**, *141*, 5402–5408.
- [24] K. Shoyama, F. Würthner, *J. Am. Chem. Soc.* **2019**, *141*, 13008–13012.

- [25] B. Pigulski, K. Shoyama, F. Würthner, *Angew. Chem. Int. Ed.* **2020**, *59*, 15908–15912; *Angew. Chem.* **2020**, *132*, 16042–16046.
- [26] A. Zhang, W. Jiang, Z. Wang, *Angew. Chem. Int. Ed.* **2020**, *59*, 752–757; *Angew. Chem.* **2020**, *132*, 762–767.
- [27] H. Zhylitskaya, J. Cybińska, P. Chmielewski, T. Lis, M. Stępień, *J. Am. Chem. Soc.* **2016**, *138*, 11390–11398.
- [28] M. Żyła-Karwowska, H. Zhylitskaya, J. Cybińska, T. Lis, P. J. Chmielewski, M. Stępień, *Angew. Chem. Int. Ed.* **2016**, *55*, 14658–14662; *Angew. Chem.* **2016**, *128*, 14878–14882.
- [29] M. Żyła-Karwowska, L. Moshniaha, Y. Hong, H. Zhylitskaya, J. Cybińska, P. J. Chmielewski, T. Lis, D. Kim, M. Stępień, *Chem. Eur. J.* **2018**, *24*, 7525–7530.
- [30] M. Navakouski, H. Zhylitskaya, P. J. Chmielewski, T. Lis, J. Cybińska, M. Stępień, *Angew. Chem. Int. Ed.* **2019**, *58*, 4929–4933; *Angew. Chem.* **2019**, *131*, 4983–4987.
- [31] L. Moshniaha, M. Żyła-Karwowska, P. J. Chmielewski, T. Lis, J. Cybińska, E. Gońka, J. Oswald, T. Drewello, S. M. Rivero, J. Casado, M. Stępień, *J. Am. Chem. Soc.* **2020**, *142*, 3626–3635.
- [32] S. Kumar, Y. K. Maurya, S. Kang, P. Chmielewski, T. Lis, J. Cybińska, D. Kim, M. Stępień, *Org. Lett.* **2020**, *22*, 7202–7207.
- [33] S. A. Balahoju, Y. K. Maurya, P. J. Chmielewski, T. Lis, M. Kondratowicz, J. Cybińska, M. Stępień, *Angew. Chem. Int. Ed.* **2022**, *61*, e202200781; *Angew. Chem.* **2022**, *134*, e202200781.
- [34] D. P. Sumy, N. J. Dodge, C. M. Harrison, A. D. Finke, A. C. Whalley, *Chem. Eur. J.* **2016**, *22*, 4709–4712.
- [35] D. P. Sumy, A. D. Finke, A. C. Whalley, *Chem. Commun.* **2016**, *52*, 12368–12371.
- [36] M. M. Boorum, Y. V. Vasil'ev, T. Drewello, L. T. Scott, *Science* **2001**, *294*, 828–831.
- [37] A. Mueller, K. Y. Amsharov, *Eur. J. Org. Chem.* **2015**, 3053–3056.
- [38] A. Tamoto, N. Aratani, H. Yamada, *Chem. Eur. J.* **2017**, *23*, 16388–16392.
- [39] R. Willstätter, E. Waser, *Ber. Dtsch. Chem. Ges.* **1911**, *44*, 3423–3445.
- [40] L. A. Paquette, *Tetrahedron* **1975**, *31*, 2855–2883.
- [41] T. Nishinaga, *Chemical Science of π -Electron Systems* (Eds.: T. Akasaka, A. Osuka, S. Fukuzumi, H. Kandori, Y. Aso), Springer Japan, Tokyo, **2015**, pp. 47–67.
- [42] K. Mouri, S. Saito, S. Yamaguchi, *Angew. Chem. Int. Ed.* **2012**, *51*, 5971–5975; *Angew. Chem.* **2012**, *124*, 6073–6077.
- [43] K. Mouri, S. Saito, I. Hisaki, S. Yamaguchi, *Chem. Sci.* **2013**, *4*, 4465.
- [44] F. Wang, X.-C. Li, W.-Y. Lai, Y. Chen, W. Huang, F. Wudl, *Org. Lett.* **2014**, *16*, 2942–2945.
- [45] M. Hada, S. Saito, S. Tanaka, R. Sato, M. Yoshimura, K. Mouri, K. Matsuo, S. Yamaguchi, M. Hara, Y. Hayashi, F. Röhricht, R. Herges, Y. Shigeta, K. Onda, R. J. D. Miller, *J. Am. Chem. Soc.* **2017**, *139*, 15792–15800.
- [46] J. Urieta-Mora, I. García-Benito, I. Zimmermann, J. Aragón, J. Calbo, G. Grancini, A. Molina-Ontoria, E. Ortí, N. Martín, M. K. Nazeeruddin, *J. Mater. Chem. C* **2019**, *7*, 6656–6663.
- [47] Z. Zhao, X. Zheng, L. Du, Y. Xiong, W. He, X. Gao, C. Li, Y. Liu, B. Xu, J. Zhang, F. Song, Y. Yu, X. Zhao, Y. Cai, X. He, R. T. K. Kwok, J. W. Y. Lam, X. Huang, D. Lee Phillips, H. Wang, B. Z. Tang, *Nat. Commun.* **2019**, *10*, 2952.
- [48] J. Urieta-Mora, M. Krug, W. Alex, J. Perles, I. Fernández, A. Molina-Ontoria, D. M. Guldi, N. Martín, *J. Am. Chem. Soc.* **2020**, *142*, 4162–4172.
- [49] M. Li, L. Yang, Y. Zhou, Y. Liu, J. Song, H. Wang, Z. Bo, *J. Phys. Chem. C* **2021**, *125*, 10841–10849.
- [50] A. Rajca, A. Safronov, S. Rajca, R. Shoemaker, *Angew. Chem. Int. Ed. Engl.* **1997**, *36*, 488–491; *Angew. Chem.* **1997**, *109*, 504–507.
- [51] S. Matsubara, Y. Koga, Y. Segawa, K. Murakami, K. Itami, *Nat. Catal.* **2020**, *3*, 710–718.
- [52] B. Ejlli, P. Nußbaum, F. Rominger, J. Freudenberg, U. H. F. Bunz, K. Müllen, *Angew. Chem. Int. Ed.* **2021**, *60*, 20220–20224; *Angew. Chem.* **2021**, *133*, 20382–20386.
- [53] T. J. Katz, *J. Am. Chem. Soc.* **1960**, *82*, 3784–3785.
- [54] Y. Zhang, Y. Zhu, D. Lan, S. H. Pun, Z. Zhou, Z. Wei, Y. Wang, H. K. Lee, C. Lin, J. Wang, M. A. Petrukhina, Q. Li, Q. Miao, *J. Am. Chem. Soc.* **2021**, *143*, 5231–5238.
- [55] Y. Zhu, Z. Zhou, Z. Wei, M. A. Petrukhina, *Organometallics* **2020**, *39*, 4688–4695.
- [56] Z. Zhou, Y. Zhu, Z. Wei, J. Bergner, C. Neiß, S. Doloczki, A. Görling, M. Kivala, M. A. Petrukhina, *Angew. Chem. Int. Ed.* **2021**, *60*, 3510–3514; *Angew. Chem.* **2021**, *133*, 3552–3556.
- [57] Z. Zhou, Y. Zhu, Z. Wei, J. Bergner, C. Neiß, S. Doloczki, A. Görling, M. Kivala, M. A. Petrukhina, *Chem. Commun.* **2022**, *58*, 3206–3209.
- [58] J. Dominikowska, M. Palusiak, *J. Comput. Chem.* **2011**, *32*, 1441–1448.
- [59] A. Yu Sokolov, D. B. Magers, J. I. Wu, W. D. Allen, P. V. R. Schleyer, H. F. Schaefer, *J. Chem. Theory Comput.* **2013**, *9*, 4436–4443.
- [60] J. Moszew, W. Żankowska-Jasińska, *Rocz. Chem.* **1958**, *32*, 225–233.
- [61] R. B. M. Ansems, L. T. Scott, *J. Am. Chem. Soc.* **2000**, *122*, 2719–2724.
- [62] M. M. Boorum, L. T. Scott, *Modern Arene Chemistry*, Wiley, Hoboken, **2002**, pp. 20–31.
- [63] Deposition Number 2161048 contains the supplementary crystallographic data for this paper. These data are provided free of charge by the joint Cambridge Crystallographic Data Centre and Fachinformationszentrum Karlsruhe Access Structures service.
- [64] T. Saji, S. Aoyagui, *J. Electroanal. Chem. Interfacial Electrochem.* **1979**, *102*, 139–141.
- [65] N. G. Connelly, W. E. Geiger, *Chem. Rev.* **1996**, *96*, 877–910.
- [66] D. Geuenich, K. Hess, F. Köhler, R. Herges, *Chem. Rev.* **2005**, *105*, 3758–3772.
- [67] Z. Chen, C. S. Wannere, C. Corminboeuf, R. Puchta, P. v. R. Schleyer, *Chem. Rev.* **2005**, *105*, 3842–3888.
- [68] L. D. Kershner, J. M. Gaidis, H. H. Freedman, *J. Am. Chem. Soc.* **1972**, *94*, 985–986.
- [69] L. Shan, D. Liu, H. Li, X. Xu, B. Shan, J.-B. Xu, Q. Miao, *Adv. Mater.* **2015**, *27*, 3418–3423.
- [70] S. H. Pun, Y. Wang, M. Chu, C. K. Chan, Y. Li, Z. Liu, Q. Miao, *J. Am. Chem. Soc.* **2019**, *141*, 9680–9686.
- [71] J. Tan, G. Zhang, C. Ge, J. Liu, L. Zhou, C. Liu, X. Gao, A. Narita, Y. Zou, Y. Hu, *Org. Lett.* **2022**, *24*, 2414–2419.

Manuscript received: May 21, 2022

Accepted manuscript online: July 12, 2022

Version of record online: August 16, 2022